Interstitial diffusion of O, N, and C in α–Ti from first-principles: Analytical model and kinetic Monte Carlo simulations

Lucia Scotti and Alessandro Mottura

Citation: J. Chem. Phys. **144**, 084701 (2016); doi: 10.1063/1.4942030
View online: http://dx.doi.org/10.1063/1.4942030
View Table of Contents: http://aip.scitation.org/toc/jcp/144/8
Published by the American Institute of Physics

Interstitial diffusion of O, N, and C in α-Ti from first-principles: Analytical model and kinetic Monte Carlo simulations

Lucia Scotti[a] and Alessandro Mottura[b]
School of Metallurgy and Materials, University of Birmingham, Birmingham B15 2TT, United Kingdom

(Received 3 November 2015; accepted 3 February 2016; published online 23 February 2016)

The high affinity of O, N, and C with α-Ti has a serious detrimental influence on the high-temperature properties of these alloys, promoting the formation of α-case. These elements dissolve in interstitial sites and diffuse very fast in α-Ti (10^3-10^8 times higher than the self-diffusivity of Ti) at high temperature accelerating the growth of α phase surface layer. Understanding the diffusion mechanisms of these elements is crucial to the design of high-temperature Ti alloys. This work aims to determine the stable interstitial sites and migration paths of O, N, and C in α-Ti. Diffusion coefficients were evaluated applying an analytical model, the multi-state diffusion method, and kinetic Monte Carlo simulations informed by first-principles calculations. The results show the reliability of these two methods with respect to the experimental data. In addition to octahedral sites, less traditional interstitial sites are shown to be stable configurations for these elements instead of tetrahedral sites. This requires to update the transition pathway networks through which these elements have been thought to migrate in α-Ti. [http://dx.doi.org/10.1063/1.4942030]

I. INTRODUCTION

The combination of low density and excellent creep behaviour of Ti alloys makes these materials desirable for aerospace applications, such as gas turbine engines. However, the low resistance against hot gas limits their upper usage temperature.[1] This detrimental phenomenon is due to the high affinity, solubility, and diffusivity of light elements, O, N, and C, in α-Ti. These elements are "α stabilisers" (i.e., they promote formation α-Ti at high temperature) and they have very high solubility values in α-Ti: 30 at. %, 19 at. % and 2 at. % at high temperature, respectively, for O, N, and C.[2] They dissolve in the interstitial sites of α-Ti, increasing the c lattice parameter and therefore c/a ratio.[2] This crystal distortion limits dislocation motion causing embrittlement and loss of ductility in Ti alloys.[2–5] In addition, these elements have high diffusion coefficients, 10^3-10^8 times higher than self-diffusivities, as shown in Fig. 1. At high temperature, they dissolve and diffuse very fast in the Ti matrix, causing the formation of very hard and brittle surface layer of α. The high diffusivity of O, N, and C has a significant effect on the growth of this phase, since the depth of alpha phase is proportional to the square root of the exposure time.[6] Understanding the migration mechanisms of these elements in α-Ti is extremely important to prevent such dangerous phenomena and design high-temperature Ti alloys.

The anisotropic character of the hcp crystal requires to perform single-crystal diffusion studies in order to fully understand the mechanism. However, obtaining a single-crystal sample is not easy. In addition, the experimental approach would not give information on fundamental aspects of the atom migration, the transition pathways. Knowing which interstitial sites O, N, and C prefer to occupy and the paths through which they migrate is a fundamental step for understanding the α phase phenomena.

In the last few decades, there has been an increasing utilisation of first-principles calculations on the study of vacancy-mediated diffusion,[7–10] as well as interstitial diffusion[11,12] in hcp crystals. In Wu and Trinkle's and O'Hara's articles,[11,12] *ab initio* calculations were used to provide data for an analytical approach called the Multi-State Diffusion (MSD) method, developed by Landman and Shlesinger,[13,14] in order to evaluate the diffusivity of interstitial elements. The results published in these articles show the reliability of Density Functional Theory (DFT) and the multi-state diffusion method.

This paper investigates the migration mechanism of O, N, and C in α-Ti using DFT together with the MSD method and kinetic Monte Carlo (KMC).

II. METHODOLOGY

In this work, the *ab initio* calculations were performed using VASP 5.3.2,[19] describing the electronic structure and exchange-correlation functional with projector augmented wave (PAW)[20] and generalised gradient approximation (GGA) parametrised by Perdew-Burke-Ernzerhof (PBE).[21] The accuracy was guaranteed using $3 \times 3 \times 3$ (54 atoms) supercell, Monkhorst-Pack mesh of $32 \times 32 \times 17$ k-points for a 2-atom cell, and energy cutoff of 350 eV.

The jump frequencies were evaluated using Eyring's definition,[22]

$$w = \nu^* \exp\left(-\frac{\Delta H_m}{k_b T}\right), \quad (1)$$

[a]Electronic mail: LXS234@bham.ac.uk
[b]Electronic mail: a.mottura@bham.ac.uk

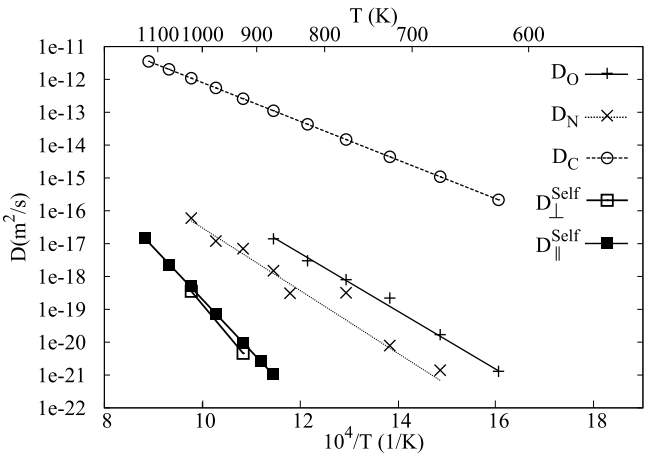

FIG. 1. Experimental bulk diffusion coefficients of O (D_O),[15] N (D_N),[16] C (D_C),[17] compared with perpendicular and parallel, $D_{\perp}^{\text{Self}}$ and $D_{\parallel}^{\text{Self}}$, self-diffusivities[18] in α-Ti.

where k_b and T are the Bolzmann's constant and absolute temperature, respectively. ΔH_m is the migration energy, defined as energy difference between the transition and initial states. The minimum energy paths were determined by climb image-nudged elastic band method (CI-NEB)[23] and improved tangent estimation[24] using 5 images between initial and final states with relaxation of ionic positions as well as shape and volume of the cells. The effective frequency ν^* was approximated using Vineyard's definition.[25]

A. Multi-state diffusion method

The multi-state diffusion method is an analytical method describing the continuous-time random walk of an atom migrating through internal states[13,14] and it can be applied to study interstitial diffusion in crystals. It consists of defining the stable interstitial sites occupied by the solute in the solvent crystal, followed by mapping the n possible jumps for each stable interstitial site. Each jump is defined by the average displacement and "waiting-time distribution" function, which describes the temporal dependence of each jump. The following step is building the Laplace transform matrix of waiting-time function, $\vec{\psi}(u)$, and Fourier transform matrix of displacement, $\underline{\tilde{p}^*}\left(\vec{k}\right)$. The diffusion variance, $\sigma_r^2(t)$, along a general direction r can be obtained solving

$$\sigma_r^2(t) = \lim_{\vec{k}\to 0} t \frac{1}{\Delta_0} \frac{\delta^2 \Delta}{\delta k_r^2}\Big|_{u\to 0}, \tag{2}$$

where Δ is the determinant of the matrix,

$$\underline{R}\left(\vec{k},u\right) = \left[I - \underline{\tilde{p}^*}\left(\vec{k}\right)\cdot\vec{\psi}(u)\right], \tag{3}$$

where I is the identity matrix, and Δ_0 is defined as

$$\Delta_0 = \lim_{u\to 0} \frac{\Delta\left(\vec{k},u\right)}{u}. \tag{4}$$

Finally, the diffusion coefficient along r is defined as,

$$D_r = \frac{\sigma_r^2(t)}{2t}. \tag{5}$$

The full matrices are provided within the supplementary material at Ref. 26.

B. Kinetic Monte Carlo

Kinetic Monte Carlo[27] is a particular Monte Carlo[28] method used for processes with known rates such as atom migration. It consists of mapping N possible events that can occur from a given state. Each event is defined by jump frequency, w_i, displacement, and cumulative function of the

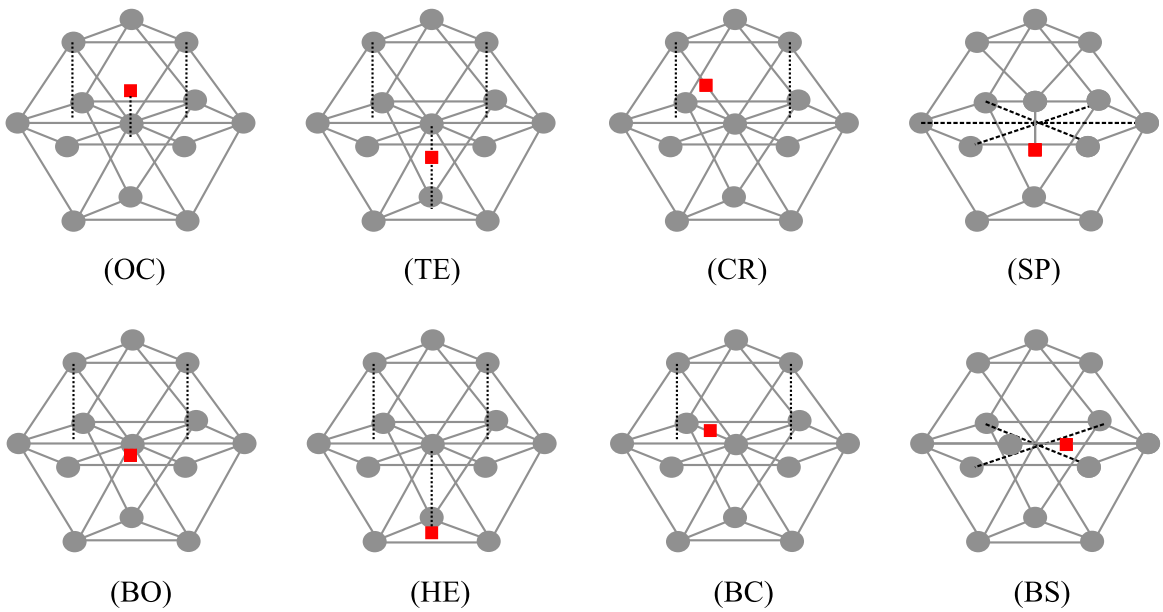

FIG. 2. Schematic representation of interstitial sites in the hcp crystal: octahedral (OC), tetrahedral (TE), crowdion (CR), split dumbbells along c axis (SP), basal octahedral (BO), hexahedral (HE), basal crowdion (BC), and split dumbbells in the basal plane (BS).

jump frequency, R_i. The main algorithm can be summarised in the following steps:

1. set initial time $t = 0$ and the initial state of the system;
2. list all N possible events and their rates w_i;
3. for each event, calculate the cumulative function R_i, defined as

$$R_i = \sum_{j=1}^{i} w_i \text{ with } i = 1, 2, \ldots, N; \tag{6}$$

4. pick a random number $u \in (0, 1]$;
5. find and perform the event i that satisfies $R_j < uR_N < R_i$;
6. pick a second random number $u' \in (0, 1]$;
7. calculate

$$\Delta t = \frac{-\ln(u')}{R_N}; \tag{7}$$

8. repeat from step 2 with the system in the new state i and $t = t + \Delta t$.

The diffusivity is defined as,

$$D = \frac{1}{2\,d}\frac{\langle r^2 \rangle}{\langle t \rangle}, \tag{8}$$

where d is the dimension of displacement vector, $\langle t \rangle$ and $\langle r^2 \rangle$ are the average time and square displacement between the initial and final positions of the species considered of n simulations. In this work, the diffusion coefficients were obtained as an average value of 100 KMC simulations of 10^6 solute jumps for each temperature.

C. Interstitial sites in hcp

There are 8 interstitial sites in hcp-crystals: octahedral (OC), tetrahedral (TE), crowdion (CR), split dumbbells along c axis (SP), basal octahedral (BO), hexahedral (HE), basal crowdion (BC), and split dumbbells in the basal plane (BS), schematically displayed in Fig. 2. The interstitial energies were calculated using,

$$E_i = E\{\mathrm{M}_N + \mathrm{I}\} - E\{\mathrm{M}_{N-1} + \mathrm{S}\} - \frac{N+1}{N}E\{\mathrm{M}_N\}, \tag{9}$$

TABLE I. Interstitial energies, E_i (eV), of O, N, and C in α-Ti. The notation in brackets indicates the interstitial position occupied after the relaxation.

	E_O (eV)	E_N (eV)	E_C (eV)
OC	−5.612	−5.931	−3.862
TE	Unstable (HE)	Unstable (HE)	Unstable (HE)
CR	−4.304	−4.554	−2.554
SP	Unstable (HE)	Unstable (HE)	Unstable (HE)
BO	Unstable	Unstable	Unstable
HE	−4.384	−4.182	Unstable
BC	Unstable (HE)	−4.610	−2.547
BS	Unstable (HE)	Unstable (BC)	Unstable (BC)

where N is the total number of solvent atoms, $E\{\mathrm{M}_N + \mathrm{I}\}$ is the energy of system where solute occupies an interstitial site, $E\{\mathrm{M}_{N-1} + \mathrm{S}\}$ is the energy of system with substitutional solute and $E\{\mathrm{M}_N\}$ is the energy of the perfect site. This energy is the energy difference between the interstitial and substitutional point defect of a given atom. A negative value of E_i indicates that the solute tends to occupy the interstitial site considered rather than sitting substitutionally within the hcp lattice.

III. RESULTS

The interstitial energies of O, N, and C in α-Ti were evaluated using DFT calculations. They are presented in Table I and displayed in Fig. 3. When the interstitial site is unstable and relaxes to a different site, the final configuration is reported in brackets in Table I. The pathway networks were mapped and calculated using CI-NEB as described in Section III A.

A. Interstitial sites in α-Ti

Oxygen stable interstitial sites are OC, HE, and CR as shown in Table I. TE, SP, BC, and BS, instead, are unstable and relax to the HE site. The basal octahedral is also unstable since it has one imaginary vibrational frequency. In the hcp unit cell, there are two equivalent OC sites, six equivalent CR sites, and two equivalent HE sites (Fig. 3(a)). The OC sites

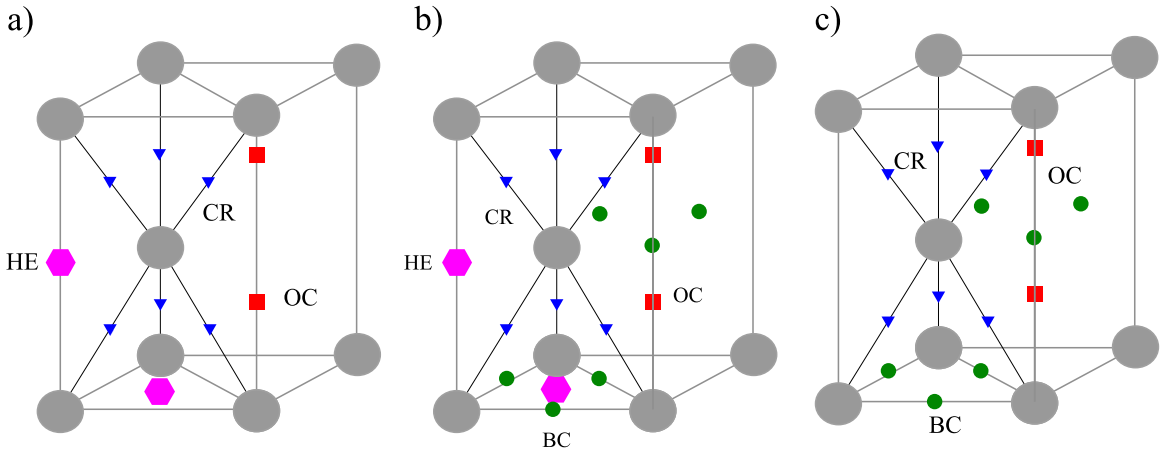

FIG. 3. Schematic representation of stable interstitial sites occupied by (a) O, (b) N, and (c) C in α-Ti unit cell.

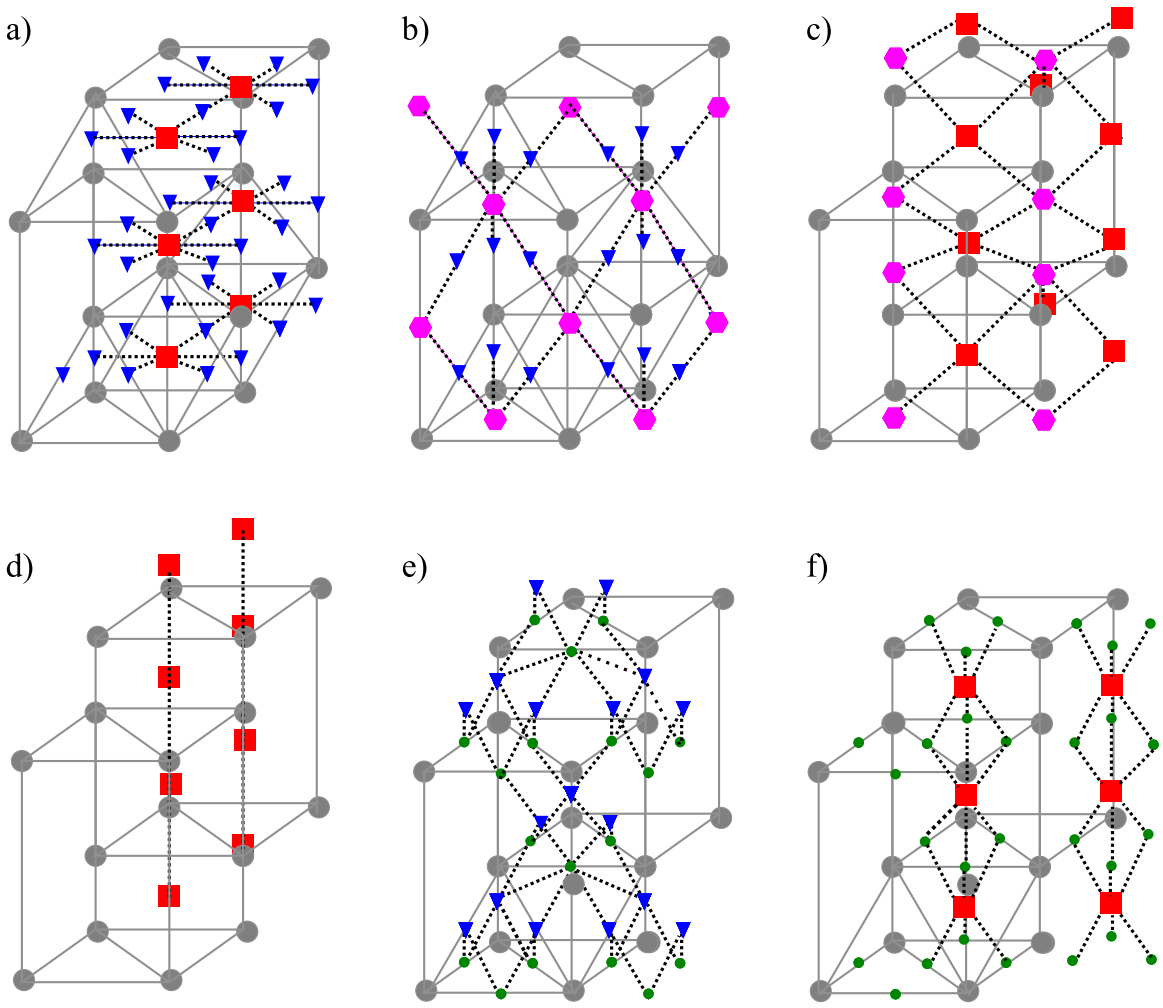

FIG. 4. Schematic representation of transition pathways between the OC, HE, BC, and CR sites in the hcp crystal: (a) OC ↔ CR, (b) HE ↔ CR, (c) OC ↔ HE, (d) OC ↔ OC along c-axis, (e) BC ↔ CR, and (f) BC ↔ OC.

are surrounded by two OC sites along the c-axis, six CR sites on the same basal plane, and six HE sites. The neighbouring sites to CR are two OC sites on the same basal plane and two HE sites. The HE sites have twelve neighbour sites: six OC and six CR sites. Therefore, from the OC sites, O can perform fourteen jumps: two OC → OC jumps, six OC → CR jumps, and six OC → HE jumps. Four jumps can be performed from CR sites: two CR → OC jumps and two CR → HE jumps. There are twelve possible jumps from HE sites: six HE → OC jumps and six HE → CR jumps. Figs. 4(a)–4(d) schematically show the pathway map of O in α-Ti. Table II summarises the migration energies and attempt frequencies of these jumps.

Similar to oxygen, nitrogen is unstable at TE, SP, and BS sites and relaxes to the HE or BC sites. BO has one imaginary frequency, hence it is also unstable. The stable sites are OC, HE, CR, and BC, as displayed in Fig. 3(b). The migration pathway network of N contains all the jumps described for O plus the transition from and to the BC sites. There are six neighbour BC positions around OC sites, leading to as many OC → BC jumps. Around CR, there are four BC sites, two on the basal plane above and two on the basal plane below, leading to four CR → BC transitions. Finally, the BC sites sit next to four CR and two OC sites: four BC → CR, and two BC → OC jumps. The BC ↔ HE jumps occur through crowdion sites. The migration pathways network of N is illustrated in Fig. 4 and Table III presents the migration energies and attempt frequencies.

Carbon is stable at OC, CR, and BC sites in α-Ti (Fig. 3(c)). HE and BO are unstable since they have an imaginary vibrational frequency. The other interstitial sites relax to other configurations (see Table I). The transition network is built with the same procedure used for O and N and are shown in Figs. 4(a) and 4(d)–4(f). When C occupies OC, it can perform two OC → OC, six OC → CR, or six OC → BC jumps. From CR sites, two CR → OC and four

TABLE II. Migration energy, ΔH_m (eV), and attempt frequency, ν (THz), of O interstitial jumps in α-Ti.

	ΔH_m (eV)	ν (THz)
OC → OC	3.850	13.67
OC → CR	1.883	27.92
OC → HE	2.061	12.24
CR → OC	0.575	11.19
CR → HE	0.596	3.60
HE → OC	0.833	10.45
HE → CR	0.676	5.70

TABLE III. Migration energy, ΔH_m (eV), and attempt frequency, ν (THz), of N interstitial jumps in α-Ti.

	ΔH_m (eV)	ν (THz)
OC → OC	3.784	18.858
OC → CR	2.038	23.217
OC → HE	2.430	10.566
OC → BC	2.164	18.181
CR → OC	0.661	20.100
CR → HE	1.093	15.098
CR → BC	1.175	12.719
HE → OC	0.682	13.237
HE → CR	0.722	9.503
BC → OC	0.842	17.367
BC → CR	1.230	35.113

CR → BC jumps are possible. Finally, from BC sites, four BC → CR and two BC → OC jumps are possible. Table IV shows the migration energies and attempt frequencies of these jumps.

B. Diffusivities of O, N, and C in α-Ti

The jump frequencies and transition networks were used to solve the MSD equation and find the diffusion coefficients. KMC simulations were also performed and used to calculate the bulk diffusion. Perpendicular and parallel diffusivities of O calculated with MSD and KMC are shown in Fig. 5. They are compared with previous *ab initio* study of Wu and Trinkle.[11] N and C diffusivities are displayed in Figs. 6 and 7, respectively. Tables V and VI contain the estimated activation energies and pre-factor diffusion coefficients for both the approaches, MSD and KMC. The diffusion within the basal plane is faster with respect to perpendicular diffusion for all atoms considered.

The results of this work for oxygen are compared to the findings of previous studies. The diffusion coefficients of O have been evaluated computationally by Wu and Trinkle[11] (Fig. 5) and experimentally by Bregolin *et al.*[15] (Fig. 8). Wu and Trinkle have evaluated interstitial sites and jump rates using VASP with ultrasoft Vanderbilt type pseudopotentials approximation[29,30] and generalised gradient approximation of Perdew and Wang[31] with ten valence electrons, energy cutoff of 400 eV, and k-point mesh of $2 \times 2 \times 2$ for 96-atom supercell and using the CI-NEB method to estimate the transition state.[11] They have evaluated $Q_\perp$ and $Q_\parallel$ to be equal to 2.084 eV and $D_{0\perp}$ and $D_{0_\parallel}$ to be equal to 2.18×10^{-8} m^2/s. Bregolin *et al.* have experimentally evaluated the bulk diffusivity using ion implantation and nuclear resonance in high-purity Ti samples (99.99%) annealed for 10 days at 1133 K in order to be able to neglect the grain-boundary diffusion and residual stress effect.[15] They have extrapolated the following bulk diffusion parameters: $Q = 1.752$ eV and $D_0 = 2 \times 10^{-7}$ m^2/s. As shown in Figs. 5 and 8, our findings are consistent with these two studies. In particular, the KMC method predicts the bulk diffusion very well. Our data match the results of Wu and Trinkle in the case of perpendicular diffusion. On the other hand, the parallel diffusivity values evaluated in this work overestimate Wu and Trinkle's values. The migration energies for CR → OC and CR → HE jumps are much smaller in the study of Wu and Trinkle: 0.28 eV and 0.24 eV, respectively. The main differences between our results and the results of Wu and Trinkle are that Wu and Trinkle performed CI-NEB calculations with a constant-shape supercells, describing the electronic structure with PAW potentials that treat 3p orbitals as valence rather than core electrons, and using a higher energy cutoff value. In order to investigate the influence of these parameters, the migration energies were calculated using the setup described in Section II with constant-shape supercells, ΔH_m^{cs}, as well as using the same energy cutoff (400 eV) and supercell size (96-atom) utilised by Wu and Trinkle allowing full relaxation, using the four-valence-electron and ten-valence electron potentials, $\Delta H_m^{400\text{-}96}$ and $\Delta H_m^{400\text{-}96\text{-}\text{pv}}$, respectively. These results are compared with the calculations of Wu and Trinkle in Table VII. The choice of higher energy cutoff and larger supercell appears to have a minor impact, since $\Delta H_m^{400\text{-}96}$ values are similar to the migration energies obtained with smaller cutoff energy and supercell (see Table II). The migration energies calculated including the additional valence electrons ($\Delta H_m^{400\text{-}96\text{-}\text{pv}}$) are closer to the results of Wu and Trinkle when compared to the results obtained without treating the 3p electrons as valence electrons ($\Delta H_m^{400\text{-}96}$). Nevertheless, the migration energies obtained keeping the supercell shape fixed (ΔH_m^{cs}) replicate the work of Wu and Trinkle well, especially in case of CR → OC and CR → HE jumps. Additionally, the choice of PAW potential has negligible effects on the defect energies of the HE and CR sites. The energy differences between the OC site and the HE and CR sites calculated with the 4s PAW are, respectively, 1.24 eV and 1.40 eV, similar to the results obtained with the 3p PAW calculations, 1.18 eV and 1.57 eV, respectively. This indicates that the discrepancies between the values of this work and the results of Wu and Trinkle are mainly due to the fact that our calculations have been performed with a full relaxation of the supercells. Due to this discrepancy, Wu and Trinkle have opted to assume that CR sites thermalise at high temperature, resulting in OC → OC jumps within the basal plane and HE → HE jumps, and a simplified equation for $D_\perp$ and $D_\parallel$. Based on the transition pathways, this approximation mostly affects the evaluation of parallel diffusion. We have tested this by replacing OC → CR → OC paths with OC → OC paths and HE → CR → HE paths with HE → HE paths in the KMC simulations, obtaining diffusivities closer to those using Wu and Trinkle's formula if inferred with the same jump frequency data (see Fig. 9).

TABLE IV. Migration energy, ΔH_m (eV), and attempt frequency, ν (THz), of C interstitial jumps in α-Ti.

	ΔH_m (eV)	ν (THz)
OC → OC	3.396	16.701
OC → CR	1.424	94.570
OC → BC	1.694	70.874
CR → OC	0.116	3.210
CR → BC	0.848	10.85
BC → OC	0.379	17.599
BC → CR	0.841	33.68

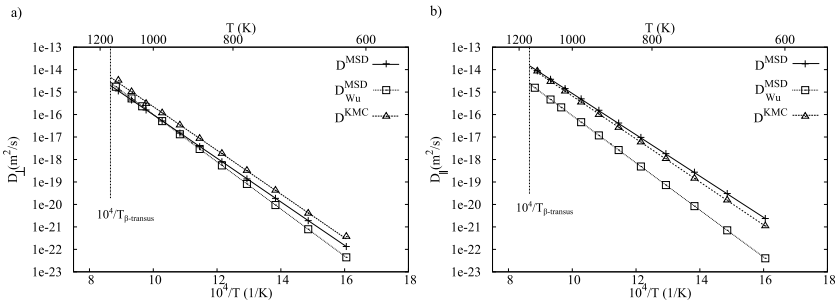

FIG. 5. Diffusion coefficients of O along (a) ⊥ and (b) ∥ directions evaluated using the MSD (D^{MSD}) and KMC method (D^{KMC}) compared with previous *ab initio* data[11] (D^{MSD}_{Wu}).

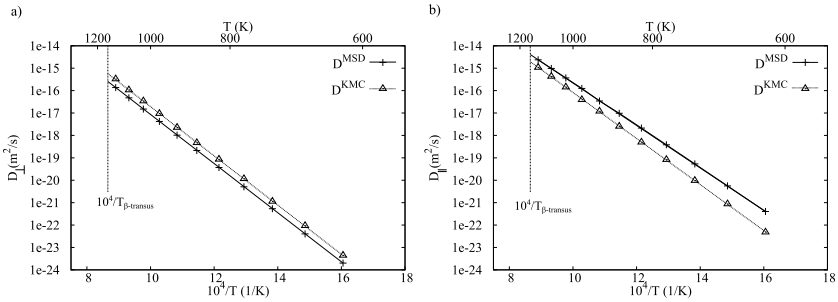

FIG. 6. Diffusion coefficients of N along (a) ⊥ and (b) ∥ directions evaluated using the MSD (D^{MSD}) and KMC method (D^{KMC}).

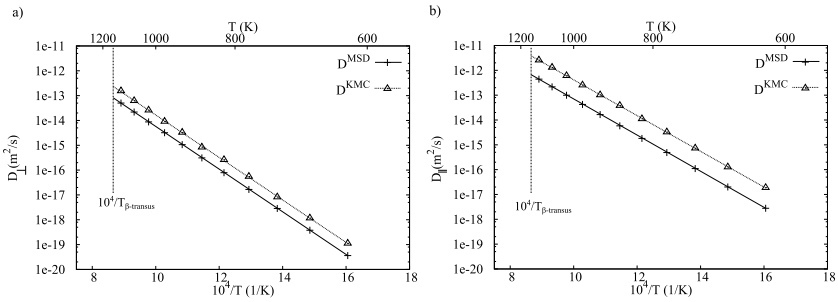

FIG. 7. Diffusion coefficients of C along (a) ⊥ and (b) ∥ directions evaluated using the MSD (D^{MSD}) and KMC method (D^{KMC}).

In the case of N and C, only experimental bulk diffusion data are available in the literature. KMC data of N bulk diffusion are compared with those obtained using ion implantation and nuclear resonance in high-purity Ti samples (99.99%)[16] in Fig. 10. Additionally, C bulk diffusion evaluated with KMC is compared with experimental values obtained using diamond deposition on pure bulk Ti substrates[17] in Fig. 11. In both cases, the KMC simulation results are consistent with the experimental values.

IV. DISCUSSION

A. Electronic structure of interstitial sites

It is a common belief that interstitial elements, such as O, N, and C, occupy octahedral and tetrahedral sites.[2] However, DFT calculations show that other interstitial sites can be occupied by these elements. Our first-principles calculations confirm previous *ab initio* findings[11,32] that O occupies octahedral and less traditional crowdion and hexahedral sites. On the other hand, tetrahedral sites are unstable and relax to hexahedral sites. Based on the interstitial energies (see Table I), O shows a preference to occupy octahedral sites. The area under the total DOS curves in Fig. 12 in the anti-bonding region (above 0 eV) is much smaller compared to the pure Ti DOS when O occupies one of the interstitial sites, especially in the case of O occupying OC and HE sites. Additionally, the Fermi energy increases when O occupies OC and HE with respect to pure Ti (3.147 eV) as shown in Table VIII. The DOS curve (Fig. 12) also reveals that the pseudo-gap at the Fermi energy is deeper when O sits at octahedral sites. These findings imply that Ti–O^{OC} and Ti–O^{HE} bonds are strong and stable with some covalent characteristics. On

TABLE V. Activation energies, Q (eV), of O, N, and C diffusion obtained using the MSD and KMC method.

	$Q^{MSD}_{\perp}$ (eV)	$Q^{MSD}_{\parallel}$ (eV)	$Q^{KMC}_{\perp}$ (eV)	$Q^{KMC}_{\parallel}$ (eV)	Q^{KMC} (eV)
O	1.923	1.825	1.930	1.899	1.903
N	2.175	1.880	2.179	2.038	2.049
C	1.705	1.444	1.697	1.428	1.431

TABLE VI. Pre-factor diffusion coefficient, D_0 (m^2/s), of O, N, and C obtained using the MSD and KMC method.

	$D^{MSD}_{0\perp}$ (m^2/s)	$D^{MSD}_{0\parallel}$ (m^2/s)	$D^{KMC}_{0\perp}$ (m^2/s)	$D^{KMC}_{0\parallel}$ (m^2/s)	D^{KMC}_{0} (m^2/s)
O	4.829×10^{-7}	1.374×10^{-6}	1.205×10^{-6}	2.485×10^{-6}	2.036×10^{-6}
N	7.914×10^{-7}	6.485×10^{-7}	1.838×10^{-6}	1.530×10^{-6}	1.295×10^{-6}
C	2.246×10^{-6}	1.336×10^{-6}	5.905×10^{-6}	6.489×10^{-6}	4.575×10^{-6}

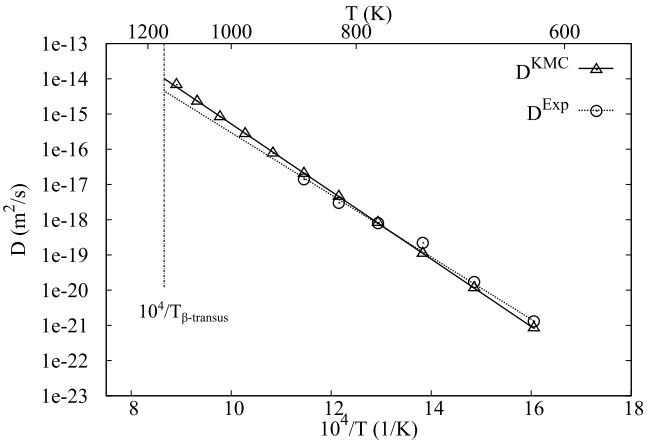

FIG. 8. Bulk diffusion coefficient of O evaluated using KMC method (D^{KMC}), compared with experimental data (D^{Exp}).[15]

TABLE VII. Comparison of migration energies of O interstitial transitions in α-Ti computed with (i) 54-atom supercells, 350 eV cutoff energy, and constant-shape relaxation (ΔH_m^{cs}), (ii) 96-atom supercells, 400 eV cutoff energy, and fully relaxed supercells, ($\Delta H_m^{400\text{-}96}$), and (iii) 96-atom supercells, 400 eV cutoff energy, fully relaxed supercells, and 3p PAW potentials ($\Delta H_m^{400\text{-}96\text{-}pv}$), with the results of Wu and Trinkle,[11] $\Delta H_m^{Wu\text{-}USPP}$ and $\Delta H_m^{Wu\text{-}PAW}$.

	ΔH_m^{cs} (eV)	$\Delta H_m^{400\text{-}96}$ (eV)	$\Delta H_m^{400\text{-}96\text{-}pv}$ (eV)	$\Delta H_m^{Wu\text{-}USPP}$ (eV)	$\Delta H_m^{Wu\text{-}PAW}$ (eV)
OC → OC	3.430	3.306	3.238	3.25	3.27
OC → CR	2.052	1.971	2.034	2.16	2.09
OC → HE	2.086	2.047	2.021	2.04	2.02
CR → OC	0.287	0.566	0.459	0.28	0.32
CR → HE	0.367	0.498	0.399	0.24	0.30
HE → OC	0.805	0.837	0.890	0.85	0.84
HE → CR	0.851	0.666	0.790	0.94	0.89

the other hand, Ti–O^{CR} is weaker showing more metallic nature.

Nitrogen shows similar behaviour, it dissolves in same sites preferred by oxygen with the addition of basal crowdion

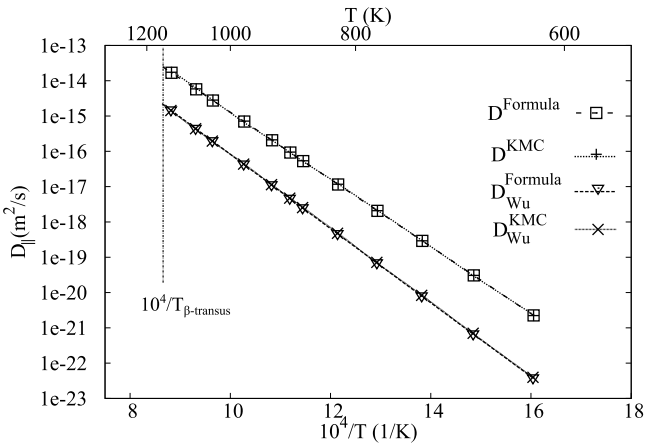

FIG. 9. Parallel diffusivity of O evaluated using Wu and Trinkle's formulation ($D^{Formula}$) and KMC simulations (D^{KMC}) neglecting CR → OC and CR → HE jumps both inferred with the jump frequency values evaluated in this work, and with Wu and Trinkle's jump frequencies data ($D^{Formula}_{Wu}$ and D^{KMC}_{Wu}).[11]

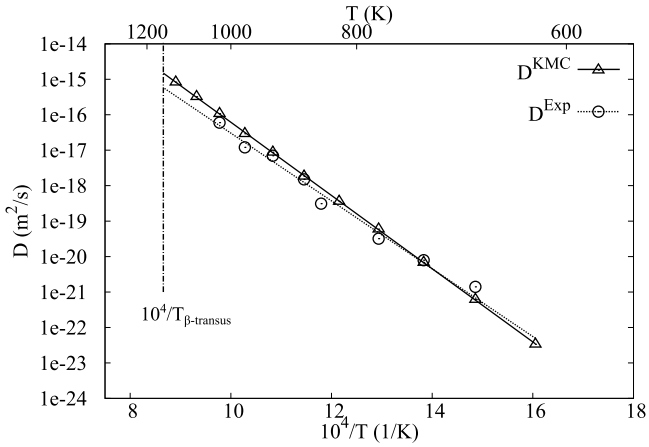

FIG. 10. Bulk diffusivity of N evaluated using KMC simulations (D^{KMC}), compared with experimental data (D^{Exp}).[16]

sites, also preferring the octahedral sites amongst all possible interstitial sites (see Table I). In the anti-bonding region of the total DOS curves (Fig. 13), the areas under Ti–N^{OC} and Ti–N^{HE} curves are narrower than Ti–N^{BC} and Ti–N^{CR}. The pseudo-gap is deeper when nitrogen occupies hexahedral and octahedral sites than when it occupies crowdion and basal crowdion sites. The Fermi energy moves to the valence region in all cases, except for when nitrogen occupies the octahedral sites (Table VIII). Ti–N^{OC} and Ti–N^{HE} bonds therefore have a covalent nature, resulting in a stronger and more stable bond compared to when nitrogen occupies the BC and CR sites.

Carbon also prefers to occupy octahedral sites like N and O; the other stable sites are crowdion and basal crowdion sites. The Ti–C^{OC} bond is more covalent than the Ti–C^{CR} and Ti–C^{BC} bonds, as shown by total DOS curves in Fig. 14. The Ti–C^{OC} DOS curve occupies a smaller portion of the anti-bonding region and its pseudo-gap is deeper. Nevertheless, C has some peculiarities when compared to N and O: the Fermi energies decrease compared to the pure Ti value (3.147 eV) when C occupies all possible interstitial sites, as shown in Table VIII. The highest energy level occupied by the Ti–C^{OC} bond in the anti-bonding zone is larger than that of N and O. Also, the area under the Ti–C^{CR} DOS curve in the anti-bonding region

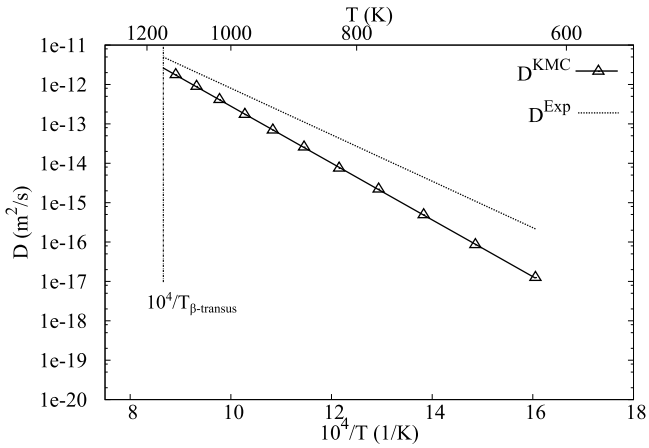

FIG. 11. Bulk diffusivity of C evaluated using KMC simulations (D^{KMC}), compared with experimental data (D^{Exp}).[17]

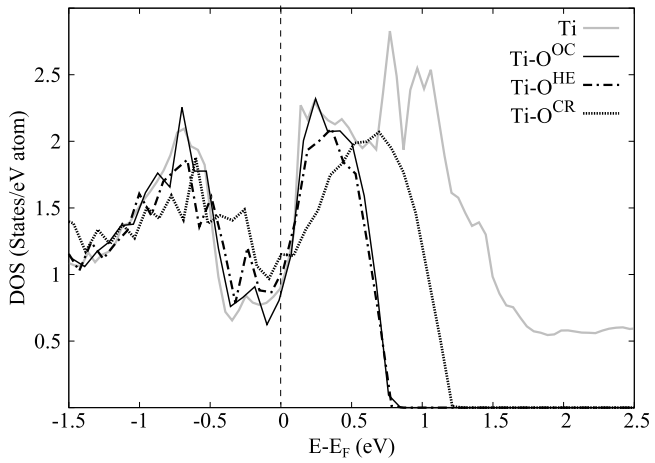

FIG. 12. Comparison of total DOS curves for pure Ti and supercells containing O at OC sites (labelled Ti–O^{OC}), HE sites (labelled Ti–O^{HE}), and CR sites (labelled Ti–O^{CR}). The energies are referred to the Fermi energies (E_F) reported in Table VIII.

TABLE VIII. Fermi energy (eV) of supercells containing O, N and C at stable interstitial sites in α-Ti.

	E_F^O (eV)	E_F^N (eV)	E_F^C (eV)
OC	3.207	3.176	3.138
CR	3.098	3.073	3.070
HE	3.167	3.141	...
BC	...	3.103	3.071

is smaller than the other two solutes. Therefore, the nature of Ti–C bond does not change between the different interstitial sites as much as it does for N and O. Ti–C^{OC} bonds are weaker when compared to the Ti–O^{OC} and Ti–N^{OC} bonds.

The detrimental influence of O, N, and C on ductility of Ti is well-documented and usually attributed to the crystal deformation induced by these solutes in the lattice.[2,33] Kwasniak and co-workers[4] have suggested that the loss of plasticity is also a result of the electronic structure of solute-solvent bonds. They have studied the influence of O addition

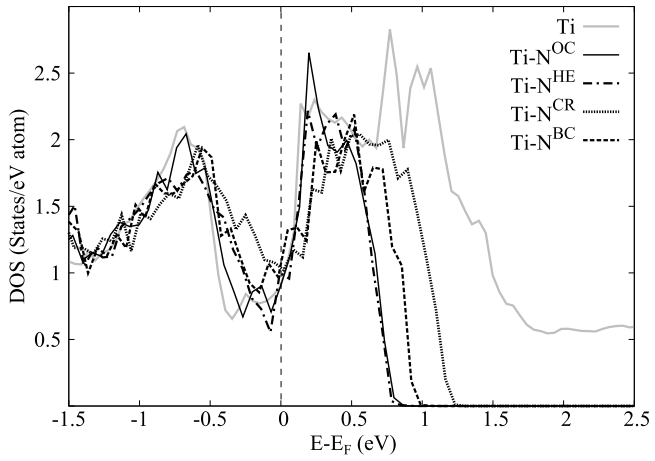

FIG. 13. Comparison of total DOS curves for pure Ti and supercells containing N at OC sites (labelled Ti–N^{OC}), HE sites (labelled Ti–N^{HE}), CR sites (labelled Ti–N^{CR}), and BC sites (labelled Ti–N^{BC}). The energies are referred to the Fermi energies (E_F) reported in Table VIII.

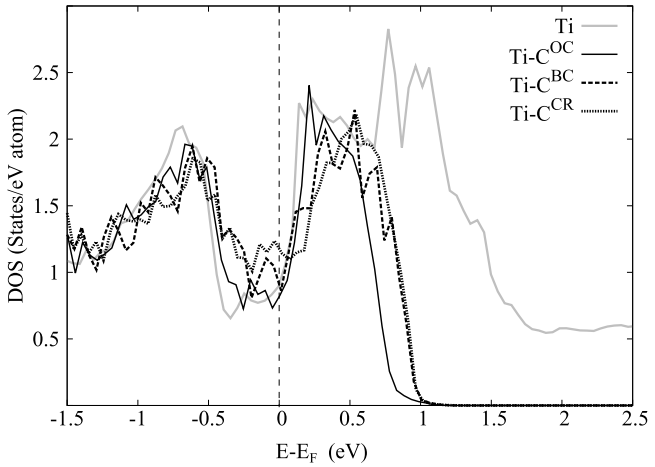

FIG. 14. Comparison of total DOS curves for pure Ti and supercells containing C at OC sites (labelled Ti–C^{OC}), CR sites (labelled Ti–C^{CR}), and BC sites (labelled Ti–C^{BC}). The energies are referred to the Fermi energies (E_F) reported in Table VIII.

on the mechanical properties and ductility of α-Ti using *ab initio*, and their results show a strong relationship between Ti–O bond nature and plasticity. They find that a higher concentration of oxygen leads to a more covalent bond, reducing the ductility. The loss of plasticity due to additions of C is less dramatic when compared to N and O; this effect can be attributed to the more metallic nature of the Ti–C bonds.[33]

B. Transition networks and anisotropy

The transition networks of O, N, and C diffusion in α-Ti were mapped using *ab initio* calculations and validated comparing KMC calculations of bulk diffusion with available experimental data. These three solutes show similar diffusion behaviours, significantly influenced by the stability of crowdion sites. The instability of tetrahedral sites significantly reduces the number of transition paths along c-axis. At the same time, the stability of crowdion sites allows jumps along $[2\bar{1}\bar{1}0]$, $[\bar{1}2\bar{1}0]$, and $[\bar{1}\bar{1}20]$ directions.

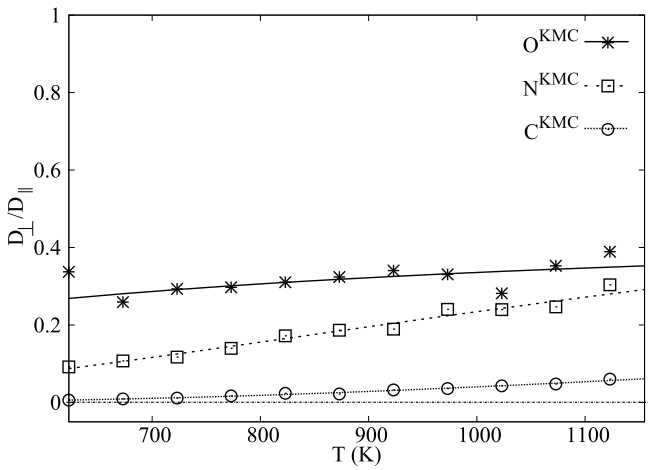

FIG. 15. Anisotropy diffusion ratio, $D_\perp/D_\parallel$, for O, N, and C in α-Ti evaluated from KMC simulations.

The OC ↔ CR jump prevails over all the other jumps, as a result of its low energy barrier. In the case of C, the migration energy of CR → OC is significantly smaller than O and N, leading to markedly higher diffusivity values. On the other hand, the high energy barrier OC ↔ OC jumps along *c*-axis, due to the instability of basal octahedral sites, increases the activation energy for perpendicular diffusion. This leads to a very high diffusion anisotropy, as shown in Fig. 15, which is accentuated for C.

V. CONCLUSIONS

In conclusion, MSD and KMC methods informed by first-principles calculations are valid and valuable instruments to study and understand the interstitial migration mechanisms in α-Ti. The diffusivity values obtained with MSD and KMC are consistent with previous *ab initio* and experimental studies. First-principles calculations show that light elements tend to occupy octahedral sites and form semi-covalent bonds with Ti, which can lead to a reduction of plasticity in Ti alloys. Also, less traditional interstitial sites are stable over tetrahedral sites: hexahedral, crowdion, and basal crowdion sites can all be occupied by these solute elements. Possible pathway networks have been mapped between these interstitial sites, showing a similar diffusion behaviour of O, N, and C. The diffusion of these elements is mainly controlled by the jump occurring between OC and CR sites within the basal plane, resulting in high diffusion anisotropy. The transition networks of these solutes lay the foundations for the control and prevention of α-case formation and growth in Ti alloys.

ACKNOWLEDGMENTS

The authors would like to acknowledge the use of the BlueBEAR High Performance Computing facility and the MidPlus Regional High Performance Computing Centre for the calculations presented in this manuscript. The authors would also like to acknowledge Timet staff for helpful discussions. Mottura acknowledges support from FP7 Marie Curie Career Integration Grant No. GA618131.

[1]C. Leyens and M. Peters, *Titanium and Titanium Alloys* (Wiley Online Library, 2003).
[2]H. Conrad, Prog. Mater. Sci. **26**, 123 (1981).
[3]A. Fitzner, J. Q. da Fonseca, M. Preuss, M. Thomas, and A. Khan, *Analytical, Computational, and Experimental Inelasticity in Deformable Solids* (NEAT, 2013), p. 4.
[4]P. Kwasniak, M. Muzyk, H. Garbacz, and K. J. Kurzydlowski, Mater. Sci. Eng. A **590**, 74 (2014).
[5]H. R. Ogden and R. I. Jaffee, "The effects of carbon, oxygen, and nitrogen on the mechanical properties of titanium and titanium alloys," Technical Report No. TML-20, Titanium Metallurgical Laboratory, Battelle Memorial Institute, Columbus, Ohio, 1955.
[6]R. W. Evans, R. J. Hull, and B. Wilshire, J. Mater. Process. Technol. **56**, 492 (1996).
[7]S. L. Shang, L. G. Hector, Jr., Y. Wang, and Z.-K. Liu, Phys. Rev. B **83**, 224104 (2011).
[8]S. Ganeshan, L. G. Hector, and Z.-K. Liu, Acta Mater. **59**, 3214 (2011).
[9]S. Ganeshan, L. G. Hector, and Z.-K. Liu, Comput. Mater. Sci. **50**, 301 (2010).
[10]D. Connétable, J. Huez, E. Andrieu, and C. Mijoule, J. Phys.: Condens. Matter **23**, 405401 (2011).
[11]H. H. Wu and D. R. Trinkle, Phys. Rev. Lett. **107**, 045504 (2011).
[12]A. O'Hara and A. A. Demkov, Appl. Phys. Lett. **104**, 211909 (2014).
[13]U. Landman and M. F. Shlesinger, Phys. Rev. B **19**, 6207 (1979).
[14]U. Landman and M. F. Shlesinger, Phys. Rev. B **19**, 6220 (1979).
[15]F. L. Bregolin, M. Behar, and F. Dyment, Appl. Phys. A **86**, 481 (2007).
[16]F. L. Bregolin, M. Behar, and F. Dyment, Appl. Phys. A **90**, 347 (2008).
[17]M. I. De Barros, D. Rats, L. Vandenbulcke, and G. Farges, Diamond Relat. Mater. **8**, 1022 (1999).
[18]M. Köppers, C. Herzig, M. Friesel, and Y. Mishin, Acta Mater. **45**, 4181 (1997).
[19]G. Kresse, M. Marsman, and J. Furthmuller, VASP the Guide, 2010.
[20]G. Kresse and D. Joubert, Phys. Rev. B **59**, 1758 (1999).
[21]J. P. Perdew, K. Burke, and M. Ernzerhof, Phys. Rev. Lett. **77**, 3865 (1996).
[22]H. Eyring, J. Chem. Phys. **3**, 107 (1935).
[23]G. Henkelman, B. P. Uberuaga, and H. Jónsson, J. Chem. Phys. **113**, 9901 (2000).
[24]G. Henkelman and H. Jónsson, J. Chem. Phys. **113**, 9978 (2000).
[25]G. H. Vineyard, J. Phys. Chem. Solids **3**, 121 (1957).
[26]See supplementary material at http://dx.doi.org/10.1063/1.4942030 for a complete description of the matrices used in the Multi-State Diffusion method applied to O, N, and C diffusion in α-Ti.
[27]J. Beeler, Jr., Phys. Rev. **150**, 470 (1966).
[28]S. Ulam, R. D. Richtmyer, and J. Von Neumann, LAMS-551, Los Alamos National Laboratory, 1947, p. 1.
[29]D. Vanderbilt, Phys. Rev. B **41**, 7892 (1990).
[30]G. Kresse and J. Hafner, J. Phys.: Condens. Matter **6**, 8245 (1994).
[31]J. P. Perdew and Y. Wang, Phys. Rev. B **45**, 13244 (1992).
[32]R. G. Hennig, D. R. Trinkle, J. Bouchet, S. G. Srinivasan, R. C. Albers, and J. W. Wilkins, Nat. Mater. **4**, 129 (2005).
[33]W. L. Finlay and J. A. Snyder, Trans. AIME **188**, 277 (1950).